RSC Advances

PAPER

View Article Online
View Journal | View Issue

Cite this: *RSC Adv.*, 2023, **13**, 31303

Photofixation of N_2 to ammonia utilizing Ni@TPP–HPA nanocomposite under visible-light illumination

Shahrbanoo Rostami, Reza Tayebee * and Behnam Mahdavi

The production of ammonia as an important raw material in the chemical, agricultural, and food industries has been always a significant concern. However, conventional ammonia production methods require high energy consumption and costs. The photocatalytic rotes use green light sources and cost-effective photocatalysts to obtain ammonia from water under aerobic conditions and preventing production of greenhouse gases in the environment. To produce an effective heterogeneous catalyst, a new tetraphenylporphyrin–heteropolyacid (TPP–HPA) nanohybrid material is synthesized and loaded onto Ni nanoparticles in this work. Then, FE-SEM, EDS, XRD, and FT-IR analyses were applied to characterize the prepared nanohybrid material Ni@TPP–HPA. After that, the new inorganic–organic nanohybrid photocatalyst was introduced as an effective, environmental friendly, and recyclable mediator for N_2 photofixation. The results showed that Ni@TPP–HPA is a good photocatalyst for the N_2 fixation reaction and can be easily recycled without losing its activity for at least five runs. The Ni@TPP–HPA nanocomposite demonstrated the maximum ammonia generation by 2760 μmol L^{-1} g^{-1} under mild conditions when using methanol as a hole scavenger. Additionally, effects of solvent type, temperature, reaction time, irradiation source, solution pH, and other electron scavengers on the rate of NH_4^+ production were investigated and discussed.

Received 12th June 2023
Accepted 18th October 2023

DOI: 10.1039/d3ra03921h

rsc.li/rsc-advances

Introduction

Ammonia (NH_3) is one of the most essential substances for all living organisms and a key component to prepare nitrogen fertilizers. Ammonia is a suitable substance for efficient and green hydrogen storage, with a global production of about 20 billion tons per year.[1] The current and widely used process for ammonia generation is the Haber–Bosch method, which requires a high temperature of 673 K, pressure above 200 bar and significant amounts of hydrogen as the starting material. Typically, 35% of the world natural gas and 14% of the world electric energy are consumed by the Haber–Bosch process.[2–4] However, the dominant Haber–Bosch generates a lot of CO_2 and consumes a lot of energy, roughly 1–2% of the worlds annual energy consumption.[5] Until now, various strategies such as electrocatalysis[6–8] and photo(electro)catalysis[5,9,10] have been adapted for N_2 reduction to NH_3. Artificial photocatalytic synthesis of ammonia from N_2 and H_2O is disclosed as a preferred and environmental friendly route for the production of NH_3. The photofixation of nitrogen to NH_3 received much attention compared to the Haber–Bosch method, because it uses solar energy directly to provide electrons and holes and combines with protons of water to reduce N_2 to NH_3.[11,12] It is a green process that does not produce CO_2 and uses little energy from the light source. Semiconductors provide photons and electrons to promote the oxidation–reduction reactions. The electrons in the valence band (VB) excite to the conduction band (CB) when energy of the irradiated light is greater than or equal to the band gap of the semiconductor material, leaving holes on the valence band and results in formation of electron–hole pairs. Nanostructures can trap electron–hole pairs and inhibit recombination of them. When these trapped electrons and holes are scattered at the surface of nanoparticles, they create a strong redox potential.[13,14]

Metalloporphyrins have a very rigid and stable coordination environment, enabling high chemical stability and strong adsorption capability, thus have been employed extensively as electrocatalysts for many reactions such as oxygen reduction reactions.[15] Towards the NRR (N_2 reduction reactions), the electron-deficient porphyrin ligands are more effective than electron-rich ones, given that nitrogen has lone pair electrons. Thus, porphyrin complexes would be prone to activate small inactive molecules such as N_2.[16,17] Heteropolyacids are also among interesting inorganic-based materials with unique properties such as good conductivity, redox activity and photocatalytic properties. For a long time, these compounds have been known as ubiquitous super-acidic catalysts and photocatalysts in a wide range of environmentally friendly synthetic routes. However, due to the good solubility of heteropolyacids

Department of Chemistry, School of Sciences, Hakim Sabzevari University, Sabzevar, Iran. E-mail: rtayebee@hsu.ac.ir

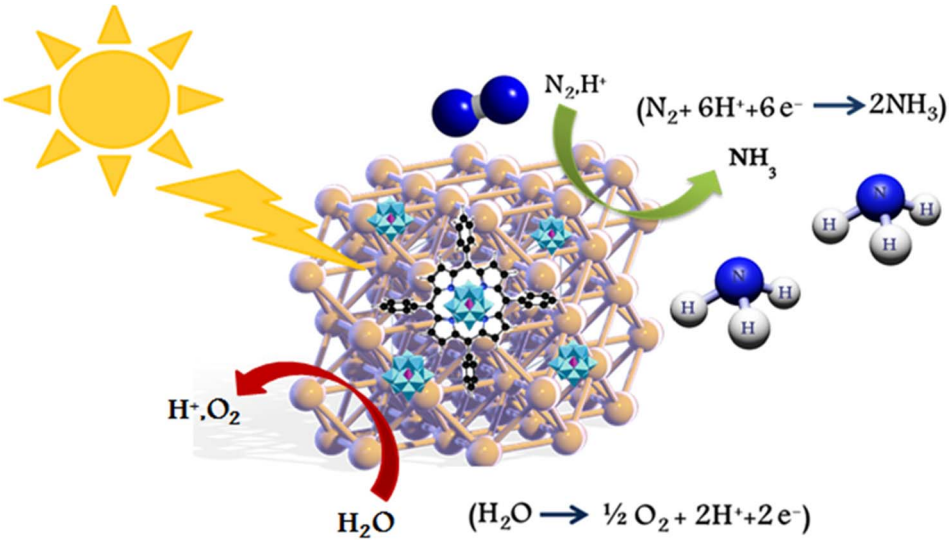

Scheme 1 A general route describing photofixation of N_2 to ammonia utilizing Ni@TPP–HPA nanocomposite under visible-light illumination.

in water and polar solvents, catalyst recycling efficiency is so low. Therefore, researchers are dedicated to effectively study grafting these compounds with other photocatalysts to fabricate an insoluble composite photocatalyst. Among heteropoly acids, the Keggin type is relatively simple and has a high super-acidic characteristic.[18] In this work, tetraphenylporphyrin and a Keggin type heteropoly acid ($H_5PW_{10}V_2O_{40}$) have contributed to attain an effective insoluble photocatalyst on nickel nanoparticles toward the target photocatalytic N_2 activation.

Herein, a new efficient heterogeneous photocatalyst is disclosed comprising tetraphenylporphyrin (TPP) and 10-tungsto-2-vanadophosphoric acid ($H_5PW_{10}V_2O_{40}$, HPA) fragments onto the Ni nanoparticles to achieve Ni@TPP–HPA nanohybrid material. The FE-SEM, EDS, FT-IR and XRD analyses were utilized to ensure preparation of the nanohybrid material. It seems that the new inorganic–organic nanohybrid photocatalyst is sufficiently effective, environmental friendly, and a recyclable mediator for N_2 photofixation under very mild conditions by using a commercial xenon irradiation source in a short time span (Scheme 1). Moreover, the photocatalyst can be easily recycled without losing its activity for at least five runs.

Experimental

Materials and methods

All chemicals involving nickel(II) nitrate hexahydrate $Ni(NO_3)_2 \cdot 6(H_2O)$, chloroform ($CHCl_3$), tetrahydrofuran (C_4H_8O), tetraphenylporphyrin ($C_{44}H_{30}N_4$), ethanol (C_2H_6O), and other solvents purchased from universal chemical companies and used as received. The heteropolyacid catalyst 10-tungsto-2-vanadophosphoric acid ($H_5PW_{10}V_2O_{40}$) prepared according to the literature.[19] Morphology studies performed using a Mira 3 XMU FE-SEM. FT-IR spectra were attained using a Shimadzu 8700 Fourier transform spectrophotometer at 400–4000 cm^{-1} with KBr pellets. XRD patterns were done on an Xpert MPD diffractometer using Cu Kα radiation at 30 mA and 40 keV with the scanning rate 3° min^{-1} in the 2θ range of 5–80°.

Preparation of nickel nanoparticles from the leaves of *Cressa cretica* extract

Preparation of the extract. The plant *Cressa cretica* was collected from North region of Rafsanjan, Iran. The leaves thoroughly washed with tap water to remove any contaminants, and then placed in a shaded area to dry completely for 10 days. After that, the dried leaves were crushed using a mortar. 10 g of the powdered dried leaves mixed with 100 mL water in a beaker. The mixture was heated to 85 °C for 25 min; then, filtered to obtain the leaf extract. The filtrate was stored at 5 °C.[20]

Synthesis of Ni NPs. In this study, nickel nanoparticles were synthesized from nickel nitrate salt and the extract of *Cressa cretica* plant. In a typical experiment for the synthesis of Ni NPs, aqueous nickel nitrate (0.06 g in 30 mL water) was added to the extract of *Cressa cretica* (10 mL, 15 g L^{-1}) with vigorous stirring, and the reaction lasted for 4 h at 60 °C. During this reaction, the chemical compounds contained in the plant extract reacted with nickel nitrate and nickel nanoparticles were formed. After the reaction, the solution was freeze-dried *in vacuo* for 24 h to obtain nickel nanoparticles.

Preparation of TPP–HPA. To prepare TPP–HPA hybrid material, the following steps were followed. At first, a solution of TPP (0.1 g) in 10 mL of THF (tetrahydrofuran) was prepared and sonicated for 15 minutes. Then, a separate solution was prepared by dissolving $H_5PW_{10}V_2O_{40}$ (0.1 g) in 13 mL of THF. This solution was also sonicated for 15 minutes to ensure proper dissolution. After that, the two solutions, containing TPP and $H_5PW_{10}V_2O_{40}$ respectively, were mixed together and sonicated for an additional 15 minutes to promote uniform dispersion and interaction between the TPP and HPA. After sonication, the resulting suspension was allowed to settle to attain a precipitate. The precipitate of TPP–HPA was dried at 65 °C for 24 hours to remove any residual solvent and ensure complete drying of the hybrid material.

Loading of TPP–HPA on Ni nanoparticles. First, 0.05 g of nickel (Ni) nanoparticles was added to 5 mL of ethanol in

a container and sonicated for 5 min to ensure complete dispersion. Then, 0.1 g of TPP–HPA was also dissolved in 10 mL of ethanol, sonicated for 5 min, and, eventually, the two suspensions were mixed and sonicated for 10 minutes to ensure proper dispersion. This step helps the uniform distribution of TPP–HPA coating on the Ni nanoparticles, preventing them from agglomerating or clumping together. Once the sonication process is complete, a precipitate was obtained and dried at 65 °C in open air for 24 hours.

Photocatalytic tests. For the purpose of investigating the photocatalytic efficacy of Ni@TPP–HPA, nitrogen fixation and conversion of N_2 to ammonia was attained. The used cell was planned simply by adopting a bilayer 100 mL glass balloon equipped with a water circulating system that absorbs UV light from the xenon lamp and allows only visible light to pass through. The catalyst (25 mg) was added to 50 mL of an aqueous solution of 20% methanol by volume. Then, nitrogen gas (>98% purity) was bubbled at the flow rate of 70 mL min^{-1}. After that, the suspension stirred for 60 min under the illumination of a commercial 1000 W xenon lamp. The concentration of ammonia was measured by spectrophotometry using Nessler's reagent.

Measurement of ammonia concentration by the Nessler's reagent. The concentration of produced ammonia was attained using the colorimetric Nessler method[21–24] as follows. After the photocatalytic reaction, the solution inside the flask was passed through a 220 nm filter. 1 mL of ammonia solution was diluted by 10 times. Then, 10 mL of the solution was transferred to the test tube involving well-mixed 0.5 mL potassium tartrate solution ($KNaC_4H_6O_6$, 0.5 mL, 500 g L^{-1}) and 0.5 mL Nessler reagent. To complete the color change, the solution was allowed to rest in a dark place for 10 min. Then, 3 mL of this solution pipetted to a quartz cuvette and absorbance was measured at 420 nm.[21] By comparing the absorbance of the unknown sample with the calibration curve (Fig. 1) obtained from known concentrations of NH_3 (prepared from ammonium chloride), the concentration of the unknown sample was determined. To check precision of the Nessler method, the indophenol blue method was also used and the obtained results were compared. Fortunately, the compared results were consistent for both methods.

Results and discussion

Ni@TPP–HPA characterization

Morphology and physicochemical characteristics of the prepared Ni@TPP–HPA nanocatalyst were investigated by FT-IR, SEM, EDS and XRD.

FT-IR

FT-IR spectroscopy is a powerful tool for determining the constituent materials of the fabricated nanophotocatalyst. The obtained spectra in the range 400–4000 cm^{-1} showed a set of functional groups, as shown in Fig. 2. This study proved presence of TPP and HPA along with Ni nanoparticles in the final nanocomposite. A broad peak at 3250–3600 cm^{-1} is due to water absorption and peaks at 3556 and 3287 cm^{-1} are related to O–H stretches. Fig. 2b shows the FT-IR spectrum of Ni@TPP–HPA. Absorption peaks from 3250 to 3600 cm^{-1} are again related to N–H and O–H vibrations. The peaks at 1300–1750 cm^{-1} are attributed to C–N, C=C and C=N bonds in tetraphenylporphyrin. Peaks at 1620 and 1348 cm^{-1} are related to C=C and C=N bonds, respectively.[25] Peaks from 700–1100 cm^{-1} are assigned to P–O, W=O, and W–O–W in the heteropolyacid. Peaks at 962 and 1080 cm^{-1} assigned to W=O stretching and tetrahedral PO_4 vibration, respectively. Peaks at 798 and 891 cm^{-1} are due to W–O–W bonds.[26]

FE-SEM

FE-SEM microscopy was used to study surface structure of the Ni@TPP–HPA nanocatalyst, as proved a nanosheet-like structure for Ni and TPP–HPA (Fig. 3). Moreover, the uniform distribution of Ni, TPP, and HPA species was observed in the surface morphology of the nanocatalyst.

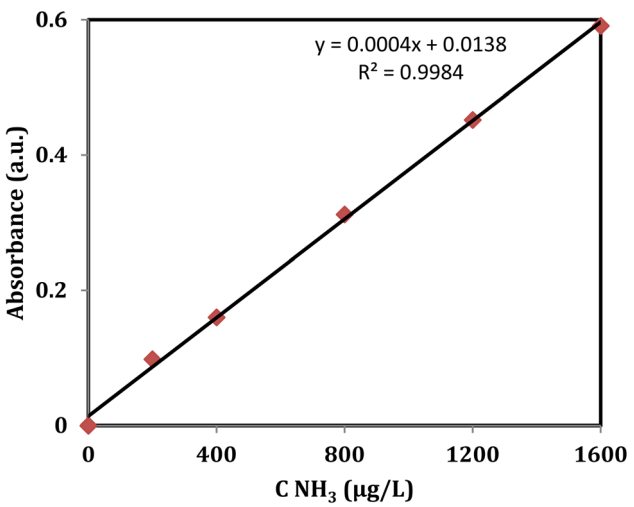

Fig. 1 Standard calibration curve for NH_3 using Nessler's reagent.

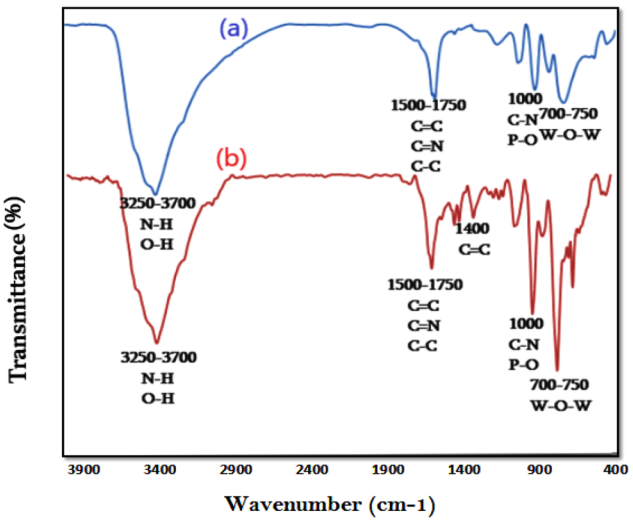

Fig. 2 FT-IR spectra of TPP–HPA (a) Ni@TPP–HPA (b).

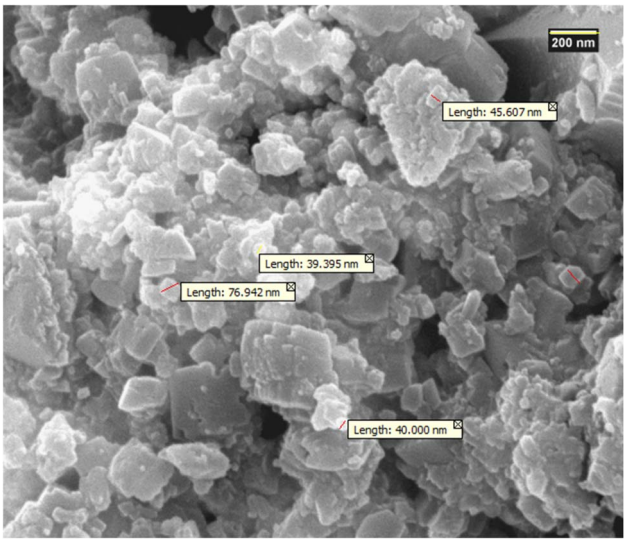

Fig. 3 The FE-SEM image of Ni@TPP–HPA.

Table 1 Atomic% and weight% for Ni@TPP–HPA based on EDS

Element	Weight%	Atomic%	Net int.
C K	20.13	52.49	78.66
N K	0.96	2.15	2.78
O K	8.87	17.36	55.78
P K	0.55	0.55	8.8
V K	1.82	1.12	36.25
Ni K	40.78	21.75	503.87
W L	26.9	4.58	105.26

EDS

The sample was subjected to EDS analysis in order to ascertain the chemical constituents of Ni@TPP–HPA (Fig. 4). An elemental analysis revealed that O, P, C, W, V, N and Ni comprise the majority of Ni@TPP–HPA (Table 1). The conversion of TPP–HPA to Ni@TPP–HPA nanocomposite was further demonstrated by this investigation.

XRD

Wide-angle XRD was used to investigate Ni, TPP–HPA, and Ni@TPP–HPA crystallinity and phases. The XRD of nickel nanoparticles in Fig. 5a reveals the fcc structure for this metal. Three characteristic peaks at 44.6°, 51.8°, and 76.5° for fcc nickel indicated the indices of (1 1 1), (2 0 0), and (2 2 2), respectively. This finding proved that the synthesized nanocrystal is pure nickel.[27] In addition, XRD pattern of TPP–HPA revealed reflections at 11.5°, 13.7°, 16.1°, 19.1°, and 28.3° due to (1 −2 1), (1 −3 1), (1 −4 1), (2 2 1), and (−1 3 3) that agree well with those of TPP.[28] The XRD pattern of $H_5PW_{10}V_2O_{40}$ showed peaks at the 2θ of 21.6°, 28.7°, 32.1°, 40.3°, 45.4°, 53.5°, 58.3° and 61.3° (Fig. 5b).[26] The diffractions for Ni@TPP–HPA observed at the 2θ of 13.5°, 20.1°, 44.7°, 51.9° and 76.6° due to the planes (1 −3 1), (221), (111), (220), and (222), indicating presence of Ni after modification with TPP and immobilization with $H_5PW_{10}V_2O_{40}$ (Fig. 5c). The slight shift in the characteristic reflections for TPP indicates that $H_5PW_{10}V_2O_{40}$ mainly occupies the TPP channels.

N_2 photofixation experiments

The molecular photosensitiser frequently fulfills the function of harvesting energy from incident light radiation in a photocatalytic system. Porphyrins are tetrapyrollic compounds that fundamentally have comparable construction as seen in chlorophyll and heme.[29] Porphyrins are planar and strongly aromatic macrocycles with 18 electrons.[30–33] An ideal photocatalytic photosensitiser should be photostable and able to absorb visible light.[32] Porphyrins are the ideal prototype for the collection of solar energy in photocatalytic reactions because they perform the same function as photosynthesis in nature.[34–36] In addition, heteropolyacids (HPAs) are semiconductor-like materials that exhibit similar properties to superacids with excellent electron acceptor capabilities and effectively promote light-generated electrons–holes separation and fast electron transfer.[37,38] HPA-based nanocomposites are recommended to remove drawbacks of heteropolyacids including low porosity, few active sites on the surface, low specific surface area, and simple solubility in polar solvents.[39–41]

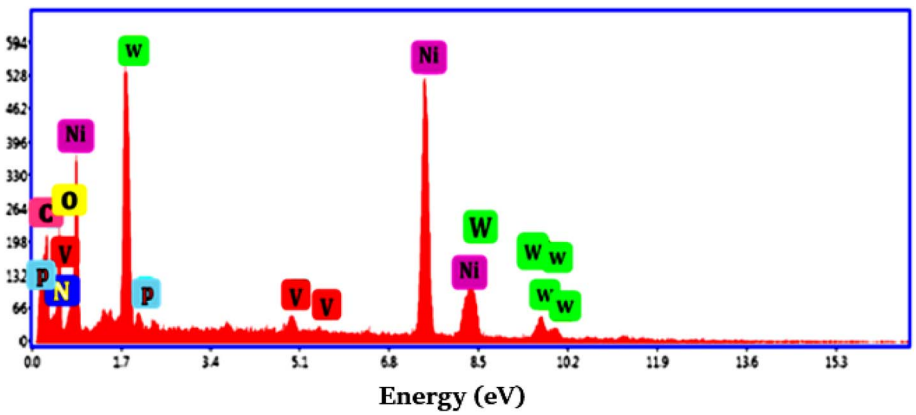

Fig. 4 EDS spectrum of Ni@TPP–HPA.

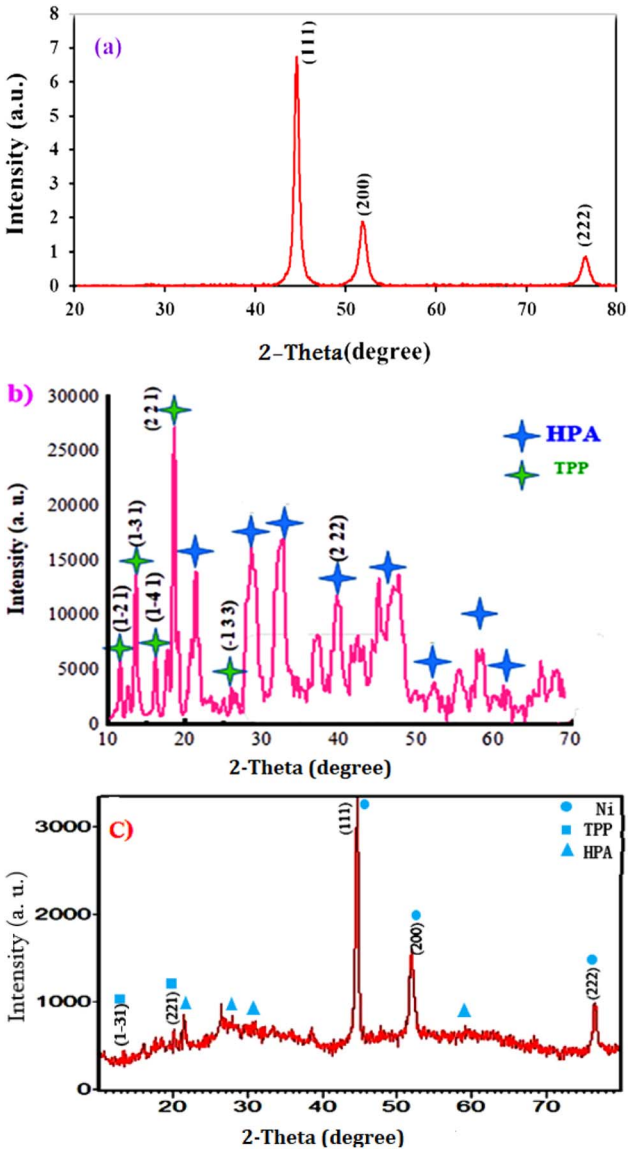

Fig. 5 Wide-angle XRD patterns of Ni (a), TPP–HPA (b) and Ni@TTP–HPA (c).

Herein, the ability of the prepared photocatalyst in the photofixation of nitrogen is performed by a commercial xenon lamp lasted for one hour and ammonia formation was measured by the Nessler method. Fig. 6 describes that photocatalyst Ni@TPP–HPA has the best photocatalytic activity compared to TPP, Ni, TPP–HPA and Ni@TPP–HPA. As can be seen, the ammonia formation rate for TPP–HPA is 1000 μmol L^{-1} g^{-1}, which is 2 times higher than that of pure TPP (470 μmol L^{-1} g^{-1}). Generally, the presence of W (tungsten) and V (vanadium) centers in the heteropolyacid compound could enhance the photocatalytic activity of the system and leading to an increase in ammonia production efficiency. These metal centers can act as active sites and facilitate conversion of dinitrogen to ammonia. Additionally, it seems that heteropolyacid could alter the electronic structure of porphyrin, promoting better adsorption and activation of nitrogen molecules. As seen in

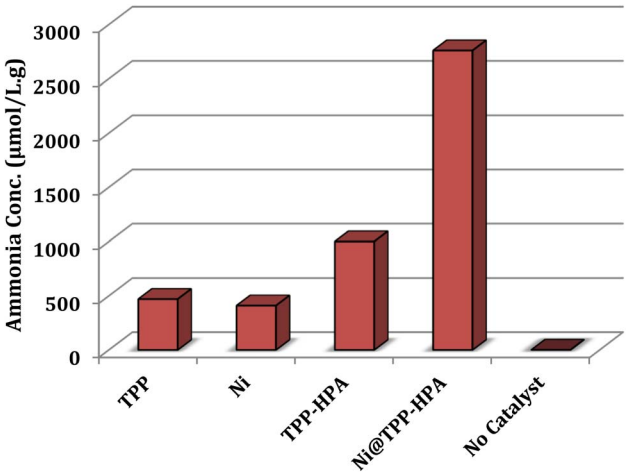

Fig. 6 Efficacy of TPP–HPA, Ni, and Ni@TPP–HPA in the N_2 photofixation. 0.025 g of photocatalyst was used in aqueous solution of 20% methanol during 60 min.

Fig. 6, presence of heteropolyacid has increased concentration of the produced ammonia from 470 to 1000 μmol g^{-1} L^{-1}. However, the specific mechanisms behind this enhanced activity would require further investigation and needs specialized equipment. The nitrogen photofixation ability of pure Ni was also investigated, and a lower activity was found (410 μmol L^{-1} g^{-1}). Fig. 6, shows that the rate of ammonia production produced by the Ni@TPP–HPA catalyst is approximately 2760, which is, respectively, 5.8, 6.7 and 2.7 times higher than that of TPP, Ni and TPP–HPA samples. Consequently, the combination of Ni with TPP–HPA has a significant effect on the nitrogen photoreduction ability. The large HOMO–LUMO band gap energy of dinitrogen (10.82 eV) seriously hinders the electron excitation processes. Therefore, it seems that interaction of N_2 to the surface Ni atoms may facilitate N–N bond dissociation.[42] However, further mechanistic investigations are needed to prove the exact role of Ni.

Influence of solvent, temperature and time

The influence of solvent type was studied (Fig. 7). The ammonia concentration was measured under the optimum conditions with some selected solvents such as deionized water, ethanol (20%), acetonitrile (20%) and 10–30% methanol.

From the results shown in Fig. 7, 20% methanol was the best between the selected solvents, yielding 2760 μmol L^{-1} g^{-1} ammonia. Commonly, CH_3OH serves as the sacrificial electron donor in most photocatalytic experiments; however, in the current photocatalysis, it seems that the proton of CH_3OH would react with N_2 more readily than that of H_2O.[43] The role of temperature was also investigated in the nitrogen fixation reaction and the temperature of 65 °C was selected as the optimum for all experiments. This investigation was carried out in the presence of 0.025 g of Ni@TPP–HPA catalyst in 20% methanol aqueous solution for 60 min. Increasing the temperature up to 65 °C resulted in an enhancement in the ammonia production efficiency; whereas, higher temperatures

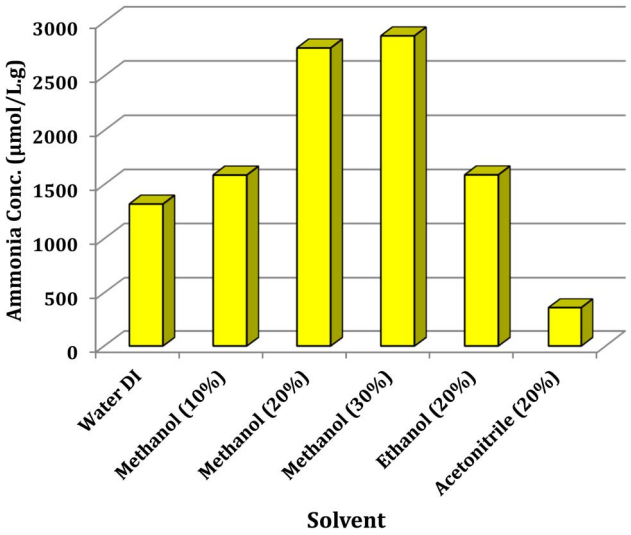

Fig. 7 Optimization of solvent type on the progress of photofixation reaction. 0.025 g of Ni@TPP–HPA was used in aqueous solution of 20% methanol during 60 min.

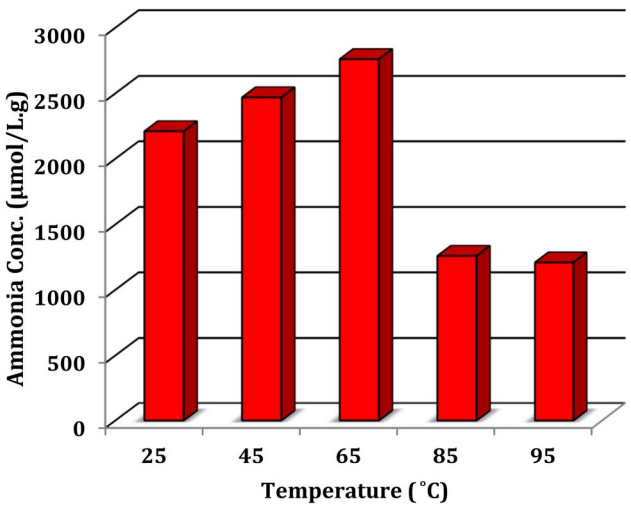

Fig. 8 Effect of temperature in the N_2 fixation. 0.025 g of Ni@TPP–HPA was used in aqueous solution of 20% methanol during 60 min.

led to a decrease in the amount of produced ammonia (Fig. 8). It can be mentioned that the reason for decreasing efficiency of NH_3 production at the high temperatures is perhaps due to agglomeration of the nanophotocatalyst particles.[44,45] Effect of reaction time was also investigated to determine the optimum time for the best yield. As can be seen in Fig. 9, the time of 60 min is sufficient to achieve the best ammonia concentration of 2760 µmol L^{-1} g^{-1}, and the lowest ammonia concentration of 935 µmol L^{-1} g^{-1} was corresponded to the reaction time of 30 min. Fig. 8 also shows effect of N_2 source. As intended, the reaction in the presence of aerobic conditions and without air bubbling led to the lowest efficacy. Whereas, bubbling of air into the solution significantly enhanced the efficacy of nitrogen photofixation. As the whole, bubbling of pure N_2 gas into the solution resulted in the best photofixation efficacy.

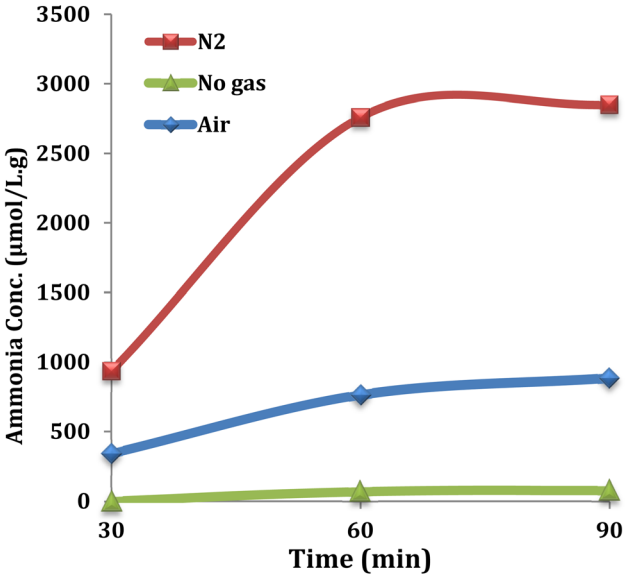

Fig. 9 Optimization of reaction time on the concentration of ammonia in the presence of 0.025 g of Ni@TPP–HPA in aqueous solution of 20% methanol at 65 °C.

Influence of the radiation source on the N_2 photofixation reaction

One of the most important factors that significantly influence the amount of ammonia production in the photocatalytic nitrogen fixation is the light source, as the results are shown in Table 2 and Fig. 10. According to this investigation, the xenon lamp produced the best efficiency with an ammonia concentration of 2760 µmol L^{-1} g^{-1}, while the least amount of ammonia (230 µmol L^{-1} g^{-1}) was attained in the absence of light source. The HP-Hg lamp is the second after xenon lamp with an ammonia production of 800 µmol L^{-1} g^{-1} and the green laser is third with an ammonia generation of 455 µmol L^{-1} g^{-1}.

The N_2 photofixation reaction was performed in the presence of 0.025 g of Ni@TPP–HPA in aqueous solution of 20% methanol at 65 °C for 60 min.

Effect of pH on the production of ammonia

To study effect of pH on the efficiency of ammonia production, pH of the reaction mixture was adjusted at the beginning of experiment by using diluted sulfuric acid and/or sodium hydroxide and the reaction was started. It should be noted that no attempt was performed to fix pH during the reaction progress, due to the fact that pH increases by producing further ammonia. The N_2 reduction in this experiment was optimized at pH 7. The results in Fig. 11 show that a decrease in pH resulted in alleviation of the photocatalytic performance, presumably because water oxidation decreases due to the increased H^+ concentration.[46,47] Increasing pH (to 10) improved water oxidation but was ineffective for NH_3 formation due to oxidation of the formed ammonia.[46] The synthesized Ni@TPP–HPA photocatalyst showed the best performance in the neutral solution due to the preservation of catalyst stability.

Table 2 Influence of light source on the N_2 photofixation reaction

Entry	Light source	Ni@TPP–HPA (g)	Time (min)	T (°C)	Ammonia conc. (μmol L^{-1} g^{-1})
1	HP-Hg 200 W, λ 200–450, 530–580 nm	0.025	60	65	800
2	25 W green laser, λ 535 nm	0.025	60	65	455
3	Xenon 1000 W, λ 420–980 nm	0.025	60	65	2760
4	Day light	0.025	60	65	230

Examining some electron/hole scavengers

The effects of several well-known electron and hole scavengers were investigated on the photocalytic reactions of nitrogen fixation and conversion to ammonia by the presence of Ni@TPP–HPA (Fig. 12). Effective species such as hydroxyl radical, holes and O_2^- anion-radical are recommended for the photocatalytic process. To prove, we used common scavengers isopropyl alcohol (IPA) to detect free hydroxyl radical.[48] The concentration was 1895 instead of 2760 μmol L^{-1} g^{-1} in the absence of IPA. In another experiment, a decrease in ammonia production (1528 μmol L^{-1} g^{-1}) was observed by the presence of *p*-benzoquinone (BQ) as O_2^- scavenger.[49] In addition, a decrease in ammonia concentration (1490 μmol L^{-1} g^{-1}) was observed by the presence of EDTA as the h^+ scavenger in the N_2

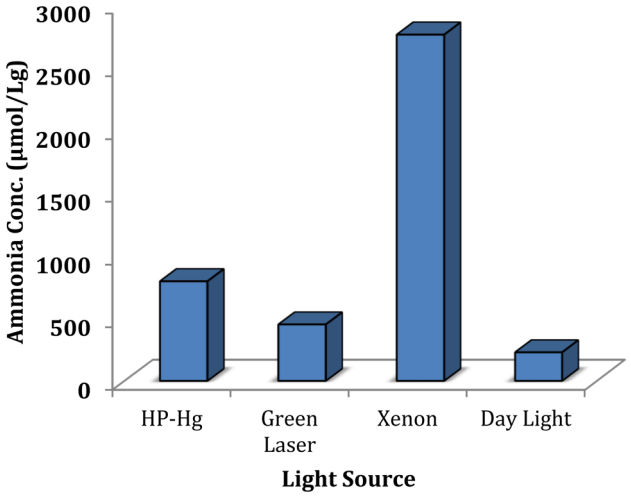

Fig. 10 Influence of the light source on the N_2 photofixation reaction. 0.025 g of Ni@TPP–HPA was used in aqueous solution of 20% methanol at 65 °C for 60 min.

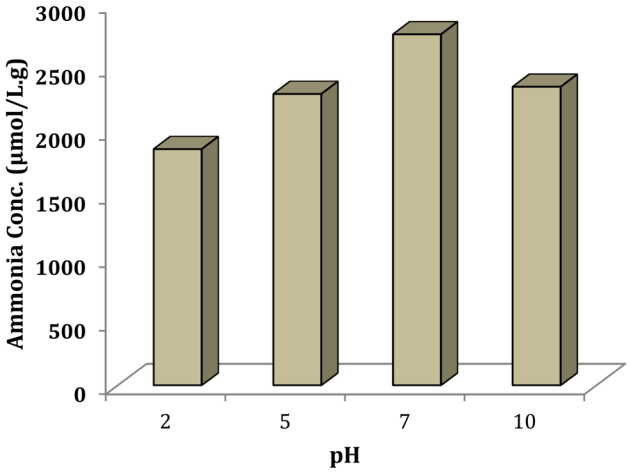

Fig. 11 Effect of pH on the generation rate of ammonia. 0.025 g of Ni@TPP–HPA was used in an aqueous solution of 20% methanol at 65 °C for 60 min.

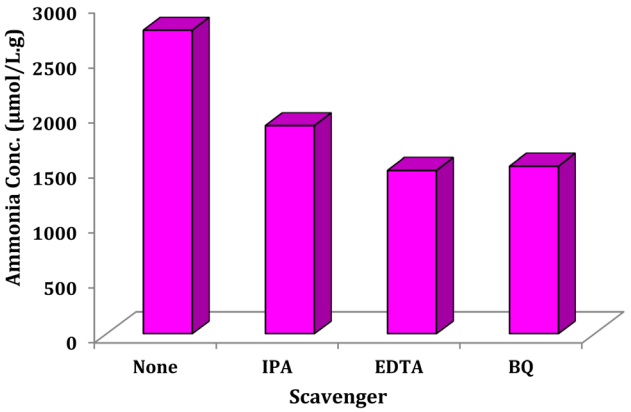

Fig. 12 Effect of some familiar scavengers on the reaction progress under the standard reaction conditions.

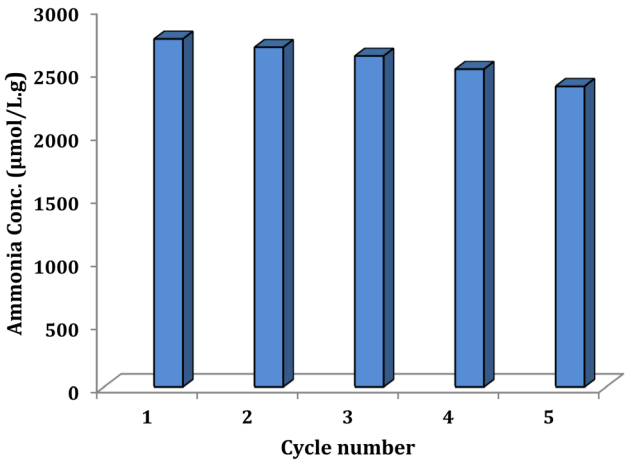

Fig. 13 Reusability of Ni@TPP–HPA nanocomposite.

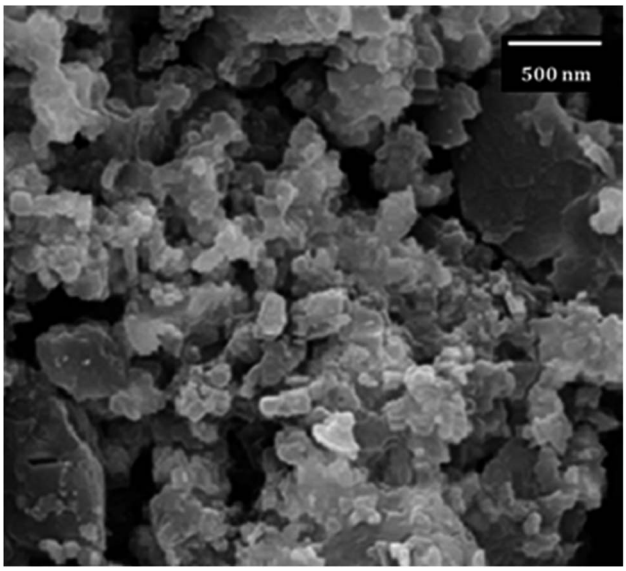

Fig. 14 SEM image of the photocatalyst after the stability test.

photofixation reaction,[50] confirming contribution of h^+. The experiments found that hydroxyl radical, hole, and superoxide anion-radical are effective species for the photocatalytic reactions. In the present study, isopropyl alcohol scavenged free hydroxyl radical. Additionally, *p*-benzoquinone as an O_2^- scavenger led to a decrease in ammonia production. Overall, these findings suggest that scavengers can have a significant impact on the photocatalytic reaction and should be considered when designing such reactions.

Investigating reusability and stability of Ni@TPP–HPA

The stability of Ni@TPP–HPA photocatalyst was determined using recycling experiments, which showed good stability of the synthesized catalyst after 5 cycles. For this purpose, after the first cycle, the nanocatalyst was separated by a simple filtration, then washed with alcohol and dried at 120 °C, and reused. The nanophotocatalyst remained stable after five cycles under the operated reaction conditions (Fig. 13). Fig. 14 shows SEM image of the nanophotocatalyst after conducting the stability test. Moreover, the FT-IR of the new and reused catalysts are compared in Fig. 15.

Effect of hydrocarbon chain-length on the ammonia production

In the photocatalytic nitrogen fixation, alcohols are used as solvent to dissolve nitrogen and serve as a source of electrons to activate the photocatalyst. The lower solubility and polarity of alcohol in water lead to the lower interaction of nitrogen and photocatalyst, which reduce the ammonia formation. In addition, as alcohol solubility in water decreases, the active surface area of the photocatalyst increases, which decreases ammonia production. Effect of the hydrocarbon chain-length of alcohol on the nitrogen photofixation was tested and analyzed, as shown in Fig. 16. The efficiency of ammonia production was decreased as the length of hydrocarbon chain increased. Fig. 16 shows that deionized water and acetonitrile solution are not suitable for this reaction and significantly reduce the photofixation efficacy.

NH_4^+ generation rate over the as-prepared photocatalyst compared to other reported mediators

The amount of ammonia production by the synthesized Ni@TPP–HPA nanocatalyst was compared with other reported mediators such as RuO_2@TiO_2–MXene,[51] Au/$Bi_2O_2CO_3$,[52] BMO/NCN,[53] and In_2O_3/In_2S_3 [54] in Table 3. It seems that Ni@TPP–HPA has several advantages including a very low amount of photocatalyst, low temperature, mild conditions and easy separation.

To determine the species of nitrate (NO_x) in the current photofixation reaction, a spectrophotometric-based method was used.[58,59] According to the performed experiment, concentration of nitrate species was found 109 μmol L^{-1} g^{-1}. Further investigation on the photocatalytic generation of nitrate species

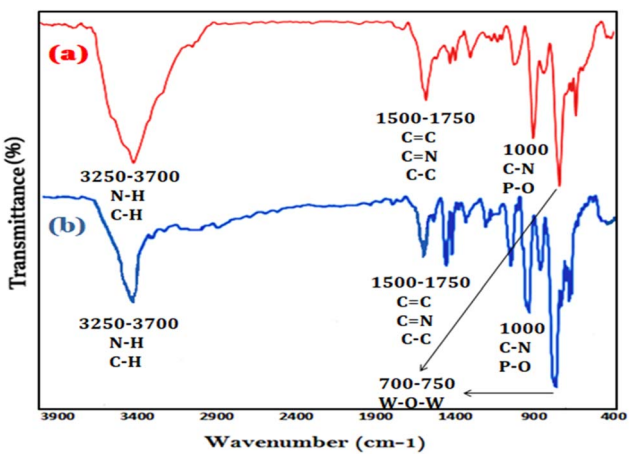

Fig. 15 FT-IR spectra of fresh Ni@TPP–HPA (a) and reused Ni@TPP–HPA (b).

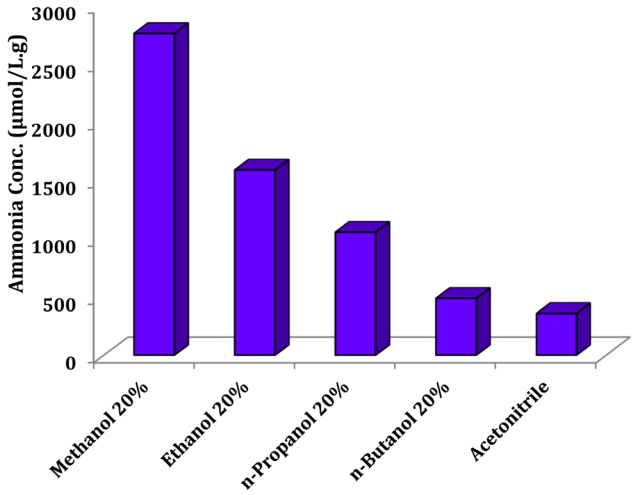

Fig. 16 Effect of hydrocarbon chain-length on the ammonia production under the optimal conditions and reaction time 60 min.

Table 3 NH_4^+ generation with Ni@TPP–HPA compared to some other reported materials

Photocatalyst	Scavenger	Light	Time (h)	Ammonia (μmol L^{-1} g^{-1})	Ref.
BMO/NCN (30%)	EtOH	Xenon 500 W	3	3271	53
Phosphated $LaFeO_3$	—	Xenon 500 W	1	1250	55
RuO_2@TiO_2–MXene	—	Xenon 300 W	7.5	450	51
$W_{18}O_{49}$/g-C_3N_4	EtOH	Xenon 300 W	4	144.1	56
Au/$Bi_2O_2CO_3$	—	Xenon 300 W	1	1910	52
Fe^{3+} doped g-C_3N_4	EtOH	Xenon 250 W (400 < λ < 800 nm)	1	299	57
In_2O_3/In_2S_3	EtOH	Xenon 300 W	1	400.4	54
Ni@TPP–HPA	MeOH	Xenon 1000 W (420 < λ < 980 nm)	1	2760	This work

is underway and the corresponding results will be published soon. The production of hydrazine in the current photcatalytic system was also estimated by the method of Watt and Chrisp.[60] The obtained results proved that hydrazine was not formed, considering detection limit of the applied procedure. At the final part of this study it should be mentioned that the mechanism involved for the current photofixation of N_2 would involve the following steps. (a) Initial light absorption by the nanocomposite and electronic excitation within the whole photocatalyst. (b) Nitrogen adsorption on the surface of photocatalyst and transfer of the excited electrons to the surface of nanoparticles. (c) Conversion of dinitrogen to ammonia *via* a series of electron transfer reactions, which promote separation of hole–electron pairs and formation of ammonia. However, detection of each step needs further attention that will be managed in recent future.

Conclusion

In this study, an efficient Ni@TPP–HPA nanophotocatalyst was fabricated by the cooperation of nickel nanoparticles, TPP, and HPA to achieve a high ammonia production of 2760 μmol L^{-1} g^{-1}. Under the optimal conditions of 60 min reaction time, 65 °C, and by using a cheap and commercial xenon lamp, the synthesized Ni@TPP–HPA nanophotocatalyst showed a high efficacy among the reported photocatalysts. The results showed that the performed photocatalyst can be easily recycled without significant loss of activity for at least five cycle. In the present study, isopropyl alcohol seems to scavenge free hydroxyl radical and *p*-benzoquinone as an O_2^- scavenger decreased ammonia production. Moreover, efficiency of ammonia production was decreased as the length of hydrocarbon chain increased and the best performance was attained under neutral conditions.

Data availability

Data that supports the findings of this study are provided throughout the text.

Conflicts of interest

On behalf of all authors, the corresponding author states that there is no conflict of interest.

Acknowledgements

The authors and creators of this work are grateful for the financial support provided by Hakim Sabzevari University. This work is also based upon research funded by Iran National Science Foundation (INSF) under project no. 4015873.

References

1 C. Guo, J. Ran, A. Vasileff and S.-Z. Qiao, Rational design of electrocatalysts and photo(electro)catalysts for nitrogen reduction to ammonia (NH_3) under ambient conditions, *Energy Environ. Sci.*, 2018, **11**, 45–56.
2 M. H. Vu, M. Sakar, S. A. Hassanzadeh-Tabrizi and T. O. Do, Photo(electro)catalytic nitrogen fixation: problems and possibilities, *Adv. Mater. Interfaces*, 2019, **6**, 1900091.
3 A. Vojvodic, A. J. Medford, F. Studt, F. Abild-Pedersen, T. S. Khan, T. Bligaard and J. Nørskov, Exploring the limits: a low-pressure, low-temperature Haber–Bosch process, *Chem. Phys. Lett.*, 2014, **598**, 108–112.
4 T. Kandemir, M. E. Schuster, A. Senyshyn, M. Behrens and R. Schlögl, The Haber-Bosch process revisited: on the real structure and stability of "ammonia iron" under working conditions, *Angew Chem. Int. Ed. Engl.*, 2013, **52**, 12723–12726.
5 A. J. Medford and M. C. Hatzell, Photon-driven nitrogen fixation: current progress, thermodynamic considerations, and future outlook, *ACS Catal.*, 2017, **7**, 2624–2643.
6 C. Guo, J. Ran, A. Vasileff and S.-Z. Qiao, Rational design of electrocatalysts and photo(electro)catalysts for nitrogen reduction to ammonia (NH_3) under ambient conditions, *Energy Environ. Sci.*, 2018, **11**, 45–56.
7 R. Li, Photocatalytic nitrogen fixation: an attractive approach for artificial photocatalysis, *Chin. J. Catal.*, 2018, **39**, 1180–1188.
8 N. Cao and G. Zheng, Aqueous electrocatalytic N_2 reduction under ambient conditions, *Nano Res.*, 2018, **11**, 2992–3008.
9 J. Li, H. Li, G. Zhan and L. Zhang, Solar water splitting and nitrogen fixation with layered bismuth oxyhalides, *Acc. Chem. Res.*, 2017, **50**, 112–121.
10 G. Schrauzer and T. Guth, Photolysis of water and photoreduction of nitrogen on titanium dioxide, *J. Am. Chem. Soc.*, 2002, **99**, 7189–7193.

11 X. Rong, H. Chen, J. Rong, X. Zhang, J. Wei, S. Liu, X. Zhou, J. Xu, F. Qiu and Z. Wu, An all-solid-state Z-scheme TiO_2/$ZnFe_2O_4$ photocatalytic system for the N_2 photofixation enhancement, *Chem. Eng. J.*, 2019, **371**, 286–293.

12 X. Chen, N. Li, Z. Kong, W.-J. Ong and X. Zhao, Photocatalytic fixation of nitrogen to ammonia: state-of-the-art advancements and future prospects, *Mater. Horiz.*, 2018, **5**, 9–27.

13 Y. Liao, J. Lin, B. Cui, G. Xie and S. Hu, Well-dispersed ultrasmall ruthenium on TiO_2 (P_{25}) for effective photocatalytic N_2 fixation in ambient condition, *J. Photochem. Photobiol., A*, 2020, **387**, 112100.

14 R. Huang, X. Li, W. Gao, X. Zhang, S. Liang and M. Luo, Recent advances in photocatalytic nitrogen fixation: from active sites to ammonia quantification methods, *RSC Adv.*, 2021, **11**, 14844–14861.

15 A. Hosseini, C. J. Barile, A. Devadoss, T. A. Eberspacher, R. A. Decreau and J. P. Collman, Hybrid bilayer membrane: a platform to study the role of proton flux on the efficiency of oxygen reduction by a molecular electrocatalyst, *J. Am. Chem. Soc.*, 2011, **133**, 11100–11102.

16 W. Zhang, W. Lai and R. Cao, Energy-related small molecule activation reactions: oxygen reduction and hydrogen and oxygen evolution reactions catalyzed by porphyrin-and corrole-based systems, *Chem. Rev.*, 2017, **117**, 3717–3797.

17 W. J. Song, M. S. Seo, S. DeBeer George, T. Ohta, R. Song, M.-J. Kang, T. Tosha, T. Kitagawa, E. I. Solomon and W. Nam, Synthesis, characterization, and reactivities of manganese(v)–oxo porphyrin complexes, *J. Am. Chem. Soc.*, 2007, **129**, 1268–1277.

18 Z. Chengli, M. Ronghua, W. Qi, Y. Mingrui, C. Rui and Z. Xiaonan, Photocatalytic degradation of organic pollutants in wastewater by heteropolyacids: a review, *J. Coord. Chem.*, 2021, **74**, 1751–1764.

19 N. MahdizadehGhohe, R. Tayebee, M. M. Amini, A. Osatiashtiani, M. A. Isaacs and A. F. Lee, $H_5PW_{10}V_2O_{40}$@VO_x/SBA-15-NH_2 catalyst for the solventless synthesis of 3-substituted indoles, *Tetrahedron*, 2017, **73**, 5862–5871.

20 Z. Wei, S. Abbaspour and R. Tayebee, Nickel Nanoparticles Originated from Cressa Leaf Extract in the Preparation of a Novel Melem@Ni-HPA Photocatalyst for the Synthesis of Some Chromenes and a Preliminary MTT Assay on the Anticancer Activity of the Nanocomposite, *Polycyclic Aromat. Compd.*, 2023, **43**, 552–571.

21 Y. Zhao, R. Shi, X. Bian, C. Zhou, Y. Zhao, S. Zhang, F. Wu, G. I. Waterhouse, L. Z. Wu and C. H. Tung, Ammonia detection methods in photocatalytic and electrocatalytic experiments: how to improve the reliability of NH_3 production rates?, *Adv. Sci.*, 2019, **6**, 1802109.

22 B. Hu, M. Hu, L. Seefeldt and T. L. Liu, Electrochemical dinitrogen reduction to ammonia by Mo_2N: catalysis or decomposition?, *ACS Energy Lett.*, 2019, **4**, 1053–1054.

23 Y.-C. Hao, Y. Guo, L.-W. Chen, M. Shu, X.-Y. Wang, T.-A. Bu, W.-Y. Gao, N. Zhang, X. Su and X. Feng, Promoting nitrogen electroreduction to ammonia with bismuth nanocrystals and potassium cations in water, *Nat. Catal.*, 2019, **2**, 448–456.

24 X. Gao, Y. Wen, D. Qu, L. An, S. Luan, W. Jiang, X. Zong, X. Liu and Z. Sun, *ACS Sustainable Chem. Eng.*, 2018, **6**, 5342–5348.

25 Z.-C. Sun, Y.-B. She, Y. Zhou, X.-F. Song and K. Li, Synthesis, characterization and spectral properties of substituted tetraphenylporphyrin iron chloride complexes, *Molecules*, 2011, **16**, 2960–2970.

26 R. Tayebee, M. M. Amini, F. Nehzat, O. Sadeghi and M. Armaghan, $H_5PW_{10}V_2O_{40}$/pyridino-SBA-15 as a highly recyclable, robust and efficient inorganic–organic hybrid material for the catalytic preparation of bis(indolyl) methanes, *J. Mol. Catal. A: Chem.*, 2013, **366**, 140–148.

27 F. Davar, Z. Fereshteh and M. Salavati-Niasari, Nanoparticles Ni and NiO: synthesis, characterization and magnetic properties, *J. Alloys Compd.*, 2009, **476**, 797–801.

28 S. Nadeem, M. A. Mutalib and M. Shima, One pot syntheses and characterization of meso-5,10,15,20-copper tetraphenylporphyrin, *Rasayan J. Chem.*, 2016, **9**, 309–314.

29 J. S. O'Neill, L. Kearney, M. P. Brandon and M. T. Pryce, Design components of porphyrin-based photocatalytic hydrogen evolution systems: a review, *Coord. Chem. Rev.*, 2022, **467**, 214599.

30 P. Sweigert, Z. Xu, Y. Hong and S. Swavey, Nickel, copper, and zinc centered ruthenium-substituted porphyrins: effect of transition metals on photoinduced DNA cleavage and photoinduced melanoma cell toxicity, *Dalton Trans.*, 2012, **41**, 5201–5208.

31 Y. Lin, T. Zhou, R. Bai and Y. Xie, Chemical approaches for the enhancement of porphyrin skeleton-based photodynamic therapy, *J. Enzyme Inhib. Med. Chem.*, 2020, **35**, 1080–1099.

32 J. Corredor, M. J. Rivero, C. M. Rangel, F. Gloaguen and I. Ortiz, Comprehensive review and future perspectives on the photocatalytic hydrogen production, *J. Chem. Technol. Biotechnol.*, 2019, **94**, 3049–3063.

33 L. Arnold and K. Müllen, Modifying the porphyrin core—a chemist's jigsaw, *J. Porphyrins Phthalocyanines*, 2011, **15**, 757–779.

34 D. Mauzerall, Porphyrins, chlorophyll, and photosynthesis, in *Photosynthesis I: Photosynthetic Electron Transport and Photophosphorylation*, 1977, pp. 117–124.

35 A. Sane and M. C. Thies, The formation of fluorinated tetraphenylporphyrin nanoparticles via rapid expansion processes: RESS vs. RESOLV, *J. Phys. Chem. B*, 2005, **109**, 19688–19695.

36 M. El-Nahass, H. Abd El-Khalek and A. M. Nawar, Topological, morphological and optical properties of gamma irradiated Ni(II) tetraphenyl porphyrin thin films, *Opt. Commun.*, 2012, **285**, 1872–1881.

37 M. S. P. Ribeiro, C. de Souza Santos, C. G. Vieira and K. A. da Silva Rocha, Catalytic transformations of (+)-aromadendrene: functionalization and isomerization reactions in the presence of the heteropoly acid catalyst $H_3PW_{12}O_{40}$, *Mol. Catal.*, 2020, **498**, 111264.

38 N. Mollakarimi Dastjerdi and M. Ghanbari, Ultrasound-promoted green approach for the synthesis of multisubstituted pyridines using stable and reusable SBA-15@ADMPT/$H_5PW_{10}V_2O_{40}$ nanocatalyst at room temperature, *Green Chem. Lett. Rev.*, 2020, **13**, 192–205.

39 K. Pamin, M. Prończuk, S. Basąg, W. Kubiak, Z. Sojka and J. Połtowicz, A new hybrid porphyrin-heteropolyacid material: synthesis, characterization and investigation as catalyst in Baeyer–Villiger oxidation. Synergistic effect, *Inorg. Chem. Commun.*, 2015, **59**, 13–16.

40 B. Maleki, E. Sheikh, E. R. Seresht, H. Eshghi, S. S. Ashrafi, A. Khojastehnezhad and H. Veisi, One-pot synthesis of 1-amidoalkyl-2-naphthols catalyzed by polyphosphoric acid supported on silica-coated $NiFe_2O_4$ nanoparticles, *Org. Prep. Proced. Int.*, 2016, **48**, 37–44.

41 M. Ghanbari, N. Mollakarimi Dastjerdi, S. Ahmadi and S. Moradi, A novel inorganic–organic nanohybrid material SBA-15@triazine/$H_5PW_{10}V_2O_{40}$ as efficient catalyst for the one-pot multicomponent synthesis of multisubstituted pyridines, *J. Iran. Chem. Soc.*, 2018, **15**, 1119–1131.

42 H.-P. Jia and E. A. Quadrelli, Mechanistic aspects of dinitrogen cleavage and hydrogenation to produce ammonia in catalysis and organometallic chemistry: relevance of metal hydride bonds and dihydrogen, *Chem. Soc. Rev.*, 2014, **43**, 547–564.

43 X. Li, X. Sun, L. Zhang, S. Sun and W. Wang, Efficient photocatalytic fixation of N_2 by KOH-treated gC_3N_4, *J. Mater. Chem. A*, 2018, **6**, 3005–3011.

44 J. He, C. Lai, L. Qin, B. Li, S. Liu, L. Jiao, Y. Fu, D. Huang, L. Li and M. Zhang, Strategy to improve gold nanoparticles loading efficiency on defect-free high silica ZSM-5 zeolite for the reduction of nitrophenols, *Chemosphere*, 2020, **256**, 127083.

45 Z. Li, M. Li, Z. Bian, Y. Kathiraser and S. Kawi, Design of highly stable and selective core/yolk–shell nanocatalysts—a review, *Appl. Catal., B*, 2016, **188**, 324–341.

46 Z. Zhao, S. Hong, C. Yan, C. Choi, Y. Jung, Y. Liu, S. Liu, X. Li, J. Qiu and Z. Sun, Efficient visible-light driven N_2 fixation over two-dimensional Sb/TiO_2 composites, *Chem. Commun.*, 2019, **55**, 7171–7174.

47 H. Hirakawa, M. Hashimoto, Y. Shiraishi and T. Hirai, Photocatalytic conversion of nitrogen to ammonia with water on surface oxygen vacancies of titanium dioxide, *J. Am. Chem. Soc.*, 2017, **139**, 10929–10936.

48 R. K. Sharma, B. Arora, S. Sharma, S. Dutta, A. Sharma, S. Yadav and K. Solanki, In situ hydroxyl radical generation using the synergism of the Co–Ni bimetallic centres of a developed nanocatalyst with potent efficiency for degrading toxic water pollutants, *Mater. Chem. Front.*, 2020, **4**, 605–620.

49 Z. Yin, M. Han, Z. Hu, L. Feng, Y. Liu, Z. Du and L. Zhang, Peroxymonosulfate enhancing visible light photocatalytic degradation of bezafibrate by Pd/g-C_3N_4 catalysts: the role of sulfate radicals and hydroxyl radicals, *Chem. Eng. J.*, 2020, **390**, 124532.

50 X. Zheng, J. Yuan, J. Shen, J. Liang, J. Che, B. Tang, G. He and H. Chen, A carnation-like rGO/$Bi_2O_2CO_3$/BiOCl composite: efficient photocatalyst for the degradation of ciprofloxacin, *J. Mater. Sci.: Mater. Electron.*, 2019, **30**, 5986–5994.

51 C. Hao, Y. Liao, Y. Wu, Y. An, J. Lin, Z. Gu, M. Jiang, S. Hu and X. Wang, RuO_2-loaded TiO_2–MXene as a high performance photocatalyst for nitrogen fixation, *J. Phys. Chem. Solids*, 2020, **136**, 109141.

52 C. Xiao, H. Hu, X. Zhang and D. R. MacFarlane, Nanostructured gold/bismutite hybrid heterocatalysts for plasmon-enhanced photosynthesis of ammonia, *ACS Sustainable Chem. Eng.*, 2017, **5**, 10858–10863.

53 E. Vesali-Kermani, A. Habibi-Yangjeh, H. Diarmand-Khalilabad and S. Ghosh, Nitrogen photofixation ability of g-C_3N_4 nanosheets/Bi_2MoO_6 heterojunction photocatalyst under visible-light illumination, *J. Colloid Interface Sci.*, 2020, **563**, 81–91.

54 H. Xu, Y. Wang, X. Dong, N. Zheng, H. Ma and X. Zhang, Fabrication of In_2O_3/In_2S_3 microsphere heterostructures for efficient and stable photocatalytic nitrogen fixation, *Appl. Catal., B*, 2019, **257**, 117932.

55 X. Sun, D. Jiang, L. Zhang, S. Sun and W. Wang, Enhanced nitrogen photofixation over $LaFeO_3$ via acid treatment, *ACS Sustain. Chem. Eng.*, 2017, **5**, 9965–9971.

56 H. Liang, H. Zou and S. Hu, Preparation of the $W_{18}O_{49}/gC_3N_4$ heterojunction catalyst with full-spectrum-driven photocatalytic N_2 photofixation ability from the UV to near infrared region, *New J. Chem.*, 2017, **41**, 8920–8926.

57 S. Hu, X. Chen, Q. Li, F. Li, Z. Fan, H. Wang, Y. Wang, B. Zheng and G. Wu, Fe^{3+} doping promoted N_2 photofixation ability of honeycombed graphitic carbon nitride: the experimental and density functional theory simulation analysis, *Appl. Catal., B*, 2017, **201**, 58–69.

58 T.-A. Bu, Y.-C. Hao, W.-Y. Gao, X. Su, L.-W. Chen, N. Zhang and A.-X. Yin, Promoting photocatalytic nitrogen fixation with alkali metal cations and plasmonic nanocrystals, *Nanoscale*, 2019, **11**, 10072–10079.

59 C. Yao, R. Wang, Z. Wang, H. Lei, X. Dong and C. He, Highly dispersive and stable Fe^{3+} active sites on 2D graphitic carbon nitride nanosheets for efficient visible-light photocatalytic nitrogen fixation, *J. Mater. Chem. A*, 2019, **7**, 27547–27559.

60 G. W. Watt and J. D. Chrisp, Spectrophotometric method for determination of hydrazine, *Anal. Chem.*, 1952, **24**, 2006–2008.